

MATERIAL DESIGN OF ANISOTROPIC ELASTIC CELLULAR BODIES WITH RESPECT TO CONTACT PROBLEM

D. J a s i ń s k a, M. J a n u s – M i c h a ł s k a

**Institute of Structural Mechanics
Cracow University of Technology
Warszawska 24, 31-155 Kraków, Poland**

Two-dimensional contact problem formulated for anisotropic, elastic bodies is considered. As an example of anisotropic medium, the cellular material is taken. The idea of two-scale modeling is adopted for formulation of an equivalent continuum, on the basis of which elastic properties can be obtained [2, 3]. Typical cellular microstructures with various types of symmetries are considered. Special attention is paid to cell structures giving negative Poisson's ratio in some directions (re-entrant cells). Application of the energy-based criterion for equivalent continuum gives macroscopic yield condition [2, 5]. Condition for the energy coefficient defined as a sum of weighted energies stored in elastic eigenstates ensures that the material works in elastic state. Unilateral frictional contact problem is analyzed using FEM. Calculations are performed for rough contact of square block subjected to normal load. Numerical solutions show differences in deformation type and contact stress distributions for different types of microstructures of the analyzed medium. The study enables the optimal choice of material structure topology, which ensures the reduction of peak contact pressure and friction stress, and applicability of anisotropic material to the given problem.

Key words: contact, friction, cellular anisotropic materials, negative Poisson's ratio.

1. INTRODUCTION

Cellular materials, with their variety of microstructures and types of material symmetries, adopted for contact problems, provide interesting topics for research. Two-scale modeling let us calculate the elastic properties of equivalent continuum on the basis of unit cell analysis. Some cell structures lead to negative Poisson's ratio in some directions. Materials with negative Poisson's ratio are called auxetic due to increasing cross-section in tension. They may be useful for a variety of applications. Among their important mechanical properties the reduction of stress concentration in contact problems shows a new area of applications. Such problem was investigated for auxetic isotropic foam [11, 12] and the results show essential differences compared with the solutions for conventional foams. For three-dimensional isotropic body limits of acceptable Poisson's ratio hold $-1 \leq \nu \leq 0.5$ as a result of thermodynamical considerations [7, 10].

For anisotropic materials these bounds are wider, theoretically they can reach infinity. The existence of directions with auxetic behaviour in cellular materials is connected with high anisotropy.

2. FORMULATION OF THE CONTACT PROBLEM

For the unilateral static contact problem of anisotropic linear elastic body with stiff and rough obstacle, the following system of equations must be fulfilled [3]:

$$(2.1) \quad \sigma_{ij,j} + f_i = 0, \quad \sigma_{ij} = S_{ijkl}\varepsilon_{kl}, \quad \varepsilon_{ij} = \frac{1}{2}(u_{i,j} + u_{j,i}) \quad \text{in } \Omega$$

completed with boundary conditions

$$(2.2) \quad u_i = \hat{u}_i \quad \text{on } \Gamma_D, \quad \sigma_{ij} \cdot n_j = t_i \quad \text{on } \Gamma_F,$$

contact conditions on Γ_C

$$(2.3) \quad \sigma_n \cdot (u_n - g) = 0, \quad \sigma_n \leq 0, \quad u_n - g \leq 0$$

and friction conditions on Γ_C

$$(2.4) \quad |\sigma_T| < \mu |\sigma_n| \Rightarrow \Delta \mathbf{u}_T = 0, \quad |\sigma_T| = \mu |\sigma_n| \Rightarrow \exists \lambda > 0; \quad \Delta \mathbf{u}_T = -\lambda \sigma_T,$$

where σ_{ij} – Cauchy stress tensor, ε_{ij} – small strain tensor, S_{ijkl} – anisotropic elastic stiffness matrix, u_i – displacement vector, f_i – body forces, \hat{u}_i – prescribed displacements on Γ_D , t_i – forces acting on Γ_F , n_i – unit normal vector, $\Gamma_D \cup \Gamma_F \cup \Gamma_C$ – boundary of the domain Ω , g – initial gap, $\sigma_n = \sigma_{ij}n_in_j$ – contact pressure, $u_n = \mathbf{u} \cdot \mathbf{n}$ – displacement normal to the boundary, $\sigma_{Ti} = \sigma_{ij} \cdot n_j - \sigma_n \cdot n_i$ – tangential contact force, and $\Delta \mathbf{u}_T = \Delta(\mathbf{u} - u_n \cdot \mathbf{n})$ – increment of tangential displacement.

To solve the boundary value problem formulated above (nonlinear due to conditions (2.3) and (2.4)), the FEM approach is used.

3. CELLULAR MICROSTRUCTURE

Cellular materials, due to a variety of material structure topology, reveal different anisotropic properties. Microstructure of material is modeled by idealized regular repeating pattern of unit cells. A skeleton of a cell is modeled as an elastic beam structure with stiff joints. The following cellular plane structures are analyzed: a) square cell structure, b) ‘honeycomb’ structure, c) equilateral triangular structure, d) ‘reentrant’ structure (giving auxetic material).

These structures represent a unit thickness layer cut from 3-dimensional material working in plane strain state. Figure 1 shows the structures mentioned above and their representative unit cells.

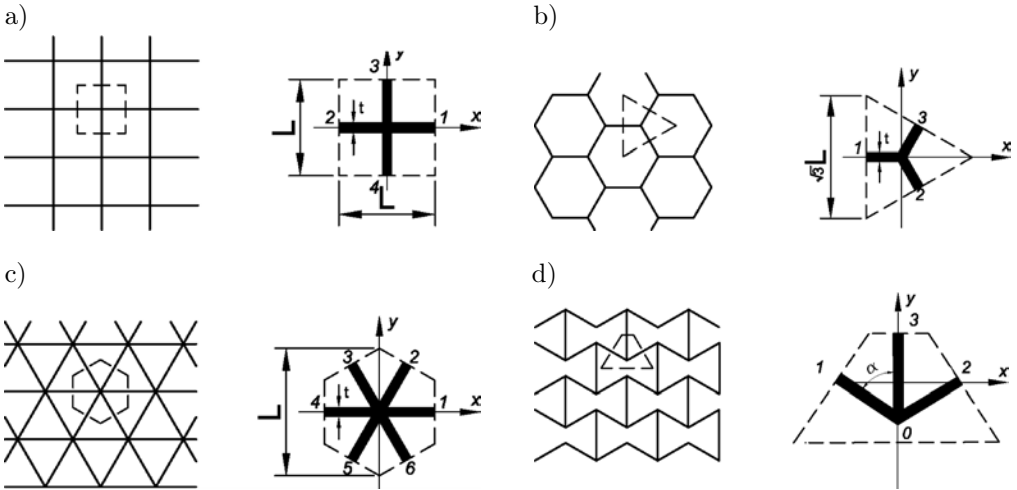


FIG. 1. Regular cellular plane structures, and their representative unit cells: a) square cell structure, square unit cell, b) 'honeycomb' structure, triangle unit cell, c) equilateral triangular structure, hexagonal unit cell, d) 'reentrant' structure, trapezoid unit cell.

Geometry of a representative unit cell can be described by midpoint position vectors: \mathbf{b}_i^0 , where $|\mathbf{b}_1^0| = h/2$, $|\mathbf{b}_i^0| = L/2$, $i = 1, 2, \dots, n$. L , h , t , γ – geometric structural parameters (for a), b), c) structures $L = h$). Skeleton material parameters are: Young's modulus – E_s , Poisson's ratio – ν_s , limit of linear elasticity – R_e .

3.1. Stiffness matrices

A framework of micromechanical modeling [2, 3, 5] is used to obtain stiffness matrices of an elastic anisotropic equivalent continuum. It starts with analyzing uniform macrostrains over the unit cell defined as follows:

$$(3.1) \quad \boldsymbol{\varepsilon} = \langle \boldsymbol{\varepsilon}^s \rangle_V = \frac{1}{V} \sum_{A_i} \text{sym} (\mathbf{n}_i \otimes \mathbf{u}_i) dS,$$

where \mathbf{u}_i – midpoint displacement vector, \mathbf{n}_i – unit normal to the cell boundary, V – volume of the representative cell, A_i – area of cell wall perpendicular to i beam.

The model assumes that macrostrains of equivalent continuum are defined by midpoint displacements of the skeleton structure. In terms of 6-D space (Kelvin notation), plane strain tensor is represented by vector $\boldsymbol{\varepsilon} = (\varepsilon_x, \varepsilon_y, \sqrt{2}\varepsilon_{xy})$ and stiffness tensor representation is a 3×3 matrix.

Given uniform unit strain fields ${}^K\tilde{\varepsilon}$, $K = 1, 2, 3$ on the unit cell, as written below:

$$(3.2)_1 \quad {}^1\tilde{\varepsilon} = (1, 0, 0), \quad {}^2\tilde{\varepsilon} = (0, 1, 0), \quad {}^3\tilde{\varepsilon} = (0, 0, \sqrt{2}),$$

the displacements for the midpoints $i = 1, 2, \dots, n$ in skeleton structure can be found:

$$(3.2)_2 \quad \Delta_i = \Delta_i({}^K\tilde{\varepsilon}), \quad i = 1, 2, \dots, n, \quad K = 1, 2, 3.$$

Next the forces normal ${}^K\tilde{F}_{in}$ and tangential ${}^K\tilde{F}_{i\tau}$ to each skeleton beam are obtained with the use of the Timoshenko beam theory. For structures a), b), and c) these are analytical solutions. For a reentrant structure d) forces are calculated numerically (using FEM ANSYS code). These forces produce stress field on macroscale (in equivalent continuum) $\tilde{\sigma}$, and on microscale (in skeleton material) $\tilde{\sigma}^s$.

For arbitrary uniform strain state represented by vector $\varepsilon = ({}^1\varepsilon, {}^2\varepsilon, {}^3\varepsilon)$, the forces can be calculated as linear combination of previous solutions as follows:

$$(3.3) \quad F_{in}(\varepsilon) = \sum_{K=1}^3 K_\varepsilon {}^K\tilde{F}_{in}, \quad F_{i\tau}(\varepsilon) = \sum_{K=1}^3 K_\varepsilon {}^K\tilde{F}_{i\tau}.$$

The definition of effective continuum assumed here is based on equivalence of the strain potential for the discrete structure and the strain potential of an equivalent continuum. It refers to averaging the strain energy density as written below:

$$(3.4) \quad \Phi_E = \langle {}^s\Phi_E \rangle_V = \frac{1}{V} \int_{V_s} ({}^s\Phi_E) dV_s,$$

where strain potential of the beam skeleton may be obtained using the following formula:

$$(3.5) \quad U = \int_{V_s} ({}^s\Phi_E) dV_s \\ = \sum_{i=1}^3 \left(\int_0^{l_i} \frac{(F_{ni})^2 d\xi_i}{2E_s A_s} + \mu \int_0^{l_i} \frac{(F_{\tau i})^2 d\xi_i}{2G_s A_s} + \int_0^{l_i} \frac{(F_{\tau i} (l_i - \xi_i))^2 d\xi_i}{2E_s J} \right),$$

where E_s , G_s – Young and shear modulus for the skeleton material, A_s , J – beam cross-sectional area and moment of inertia, μ – energy cross-sectional coefficient (for rectangular cross-section $\mu = 1.2$).

Due to linearity of the stress-strain relationship, the strain energy density function is represented by the following quadratic form:

$$(3.6) \quad \Phi_E = \frac{1}{2} \boldsymbol{\varepsilon} : \mathbf{S} : \boldsymbol{\varepsilon}.$$

Introducing relation (3.3) to the expression of strain potential and differentiating it with respect to macrostrain components as follows:

$$(3.7) \quad S_{IJ} = \frac{1}{V} \left(\int_{V_s} \frac{\partial^2 ({}^S \Phi_E)}{\partial ({}^I \boldsymbol{\varepsilon}) \partial ({}^J \boldsymbol{\varepsilon})} dV_s \right),$$

one obtains the formula for stiffness matrix components of an anisotropic equivalent continuum.

These components can be obtained as a result of a procedure based on Eqs. (3.1)–(3.4) and (3.6)–(3.7) [2].

3.2. Poisson's ratio and other material properties

Typical cellular structures with honeycomb and triangular shape of skeleton give always positive Poisson's ratio values in each direction in plane since they represent transversal symmetry. For isotropy in two-dimensional problems, limits of acceptable Poisson's ratio become $-1 \leq \nu \leq 1$ due to thermodynamical considerations [9]. The honeycomb structure is more compliant and Poisson's ratio can attain greater value, but limited by relation $\nu \leq 1$. The triangular structure shape is stiff and gives lower Poisson's ratio. The value of Poisson's ratio for the symmetries mentioned above is constant; it means that it is independent of the direction of tension. This constant is dependent on geometric and material microstructural parameters as given in Appendix B. Square structure gives anisotropic material with zero Poisson's ratio in symmetry axis. In other directions the value is limited by relation $0 \leq \nu \leq 1$. Generally for greater cellular material density of fixed microstructure type, the Poisson's ratio value is lower than for lower density. Some skeleton geometries lead to nonpositive Poisson's ratio. For instance, a honeycomb with inverted hexagonal cells leads to negative Poisson's ratio in some directions. This unusual characteristics is achieved by forming the cells into re-entrant shape, which bulges inwards and which unfolds under tension resulting in a lateral expansion [6]. Detailed study of directional properties of cellular material with re-entrant honeycomb structure in dependence on microstructural parameters is given in [2].

Graphical representation of chosen material properties for material structures a), b), c), d) with geometric and skeleton material data used for numerical examples are given in Appendix B.

Evaluation of cellular material properties decides on the applicability of the material to the given problem.

3.3. Assessment of elastic range

Majority of cellular materials reveal nonlinear behavior. Although linear analysis gives only estimation of elastic limits, it enables to predict applicability of chosen microstructure to material design.

Matrix representation of stiffness tensor for plane structures in Kelvin's notation in 6-D space is as follows:

$$(3.8) \quad \mathbf{S} = \begin{bmatrix} S_{11} & S_{12} & S_{13} \\ S_{12} & S_{22} & S_{23} \\ S_{13} & S_{23} & S_{33} \end{bmatrix}.$$

In general this matrix has three eigenvalues: λ_I , λ_{II} , λ_{III} , and the corresponding stiffness matrix eigenstrains:

$${}^I\tilde{\boldsymbol{\varepsilon}} = ({}^I\tilde{\varepsilon}_x, {}^I\tilde{\varepsilon}_y, {}^I\tilde{\varepsilon}_{xy}), \quad {}^{II}\tilde{\boldsymbol{\varepsilon}} = ({}^{II}\tilde{\varepsilon}_x, {}^{II}\tilde{\varepsilon}_y, {}^{II}\tilde{\varepsilon}_{xy}), \quad {}^{III}\tilde{\boldsymbol{\varepsilon}} = ({}^{III}\tilde{\varepsilon}_x, {}^{III}\tilde{\varepsilon}_y, {}^{III}\tilde{\varepsilon}_{xy})$$

or stiffness matrix eigenstresses:

$$(3.9) \quad {}^I\tilde{\boldsymbol{\sigma}} = \lambda_I {}^I\tilde{\boldsymbol{\varepsilon}}, \quad {}^{II}\tilde{\boldsymbol{\sigma}} = \lambda_{II} {}^{II}\tilde{\boldsymbol{\varepsilon}}, \quad {}^{III}\tilde{\boldsymbol{\sigma}} = \lambda_{III} {}^{III}\tilde{\boldsymbol{\varepsilon}}.$$

Equations (3.1)–(3.4) enable to calculate the forces in skeleton structure for strain eigenstates and to formulate the limit condition for bending and tension in the skeleton in the form:

$$(3.10) \quad \max_i ({}^\alpha\sigma_x^s) = R_e, \quad \alpha = I, II, III, \quad i = 1, 2, \dots, n.$$

The coefficients defined as follows:

$$(3.11) \quad k_\alpha := \frac{R_e}{\alpha\tilde{\sigma}_x^s} \quad \alpha = I, II, III$$

are obtained as a result of analytical considerations or numerical calculations. Analytical formulae for these coefficients depending on geometric structural and skeleton material parameters for structures a), b), c) are given in Appendix A. For structure d) these coefficient are obtained as a result of numerical calculations.

Limit eigenstrains and eigenstresses are as follows:

$$(3.12) \quad {}^\alpha\boldsymbol{\varepsilon}^{\text{gr}} = k_\alpha {}^\alpha\tilde{\boldsymbol{\varepsilon}}, \quad {}^\alpha\boldsymbol{\sigma}^{\text{gr}} = \lambda_\alpha {}^\alpha\boldsymbol{\varepsilon}^{\text{gr}}, \quad \alpha = I, II, III.$$

The analysis presented above lets us also predict deformability of the given material in elastic range. It can be described as maximum elongation in the x , y direction or shear angle in the xy plane, which reads as follows:

$$(3.13) \quad \max |\varepsilon_x| = \sum_{\alpha=1}^{\text{III}} |\varepsilon_x^{\text{gr}}|, \quad \max |\varepsilon_y| = \sum_{\alpha=1}^{\text{III}} |\varepsilon_y^{\text{gr}}|, \quad \max |\varepsilon_{xy}| = \sum_{\alpha=1}^{\text{III}} |\varepsilon_{xy}^{\text{gr}}|.$$

3.4. Energy-based yield criterion for anisotropic continuum

For an arbitrary anisotropic solid, the energy-based Rychlewski criterion [13] is formulated in the form of a sum of weighted energies stored in eigenstates of anisotropy stiffness tensor as follows:

$$(3.14) \quad \sum_{\alpha=1}^{\text{III}} \frac{\alpha \Phi_E}{\alpha \Phi_E^{\text{gr}}} = 1,$$

where $\alpha \Phi_E^{\text{gr}}$ is the critical energy for α state, $\alpha = \text{I, II, III}$.

Energy-based yield criterion is a type of energy hypothesis for cellular material. The subject of investigation is the limit state of linear elasticity which corresponds to the first yield point in the skeleton structure. Such an approach was successively adopted to a cellular 3D structured material [3, 5] and foams. It shows a good agreement with experimental data [5].

Critical energies in Eq. (3.14) can be calculated by means of the formula:

$$(3.15) \quad \alpha \Phi_E^{\text{gr}} = \frac{1}{2} \alpha \boldsymbol{\sigma}^{\text{gr}} \cdot \alpha \boldsymbol{\varepsilon}^{\text{gr}} = \frac{1}{2} \lambda_{\alpha} k_{\alpha}^2 \alpha \tilde{\varepsilon}^2.$$

The criterion presented above gives macroscopic yield condition for arbitrary stress state, in particular for uniaxial tension, which is important due to the fact that it can be compared with experimental results. For the considered structures a), b), c), the formulae depending on skeleton material parameters and geometric parameters of skeleton structures are given in Appendix A. For structure d) these energies are obtained numerically.

The elastic stiffness matrix (3.8), yield stresses and limit strains (3.12), (3.13) describing deformability in the elastic range, depend on material properties of a solid phase of the cell and topological arrangement of its structure. Detailed study of material properties depending on structural parameters is given in [2, 3].

3.5. Material strength in arbitrary plane stress state

The considered contact problem is linearly elastic. To conform this requirement it is necessary to introduce a measure of material strength in arbitrary

point of the material and give the range of this measure for elasticity. The consequence of the adopted form of yield criterion is the choice of energy coefficient defined as a sum of weighted energies stored in subsequent eigenstates as written below:

$$(3.16) \quad \varphi = \sum_{\alpha=1}^{\text{III}} \frac{\alpha \bar{\Phi}_E}{\alpha \bar{\Phi}_E^{\text{gr}}}.$$

In the limit state the coefficient reaches its maximum value $\varphi = 1$. Critical energies can be defined as structural parameters of the material strength.

For generality of considerations we assume arbitrary orientation of cellular x, y axes with respect to global X, Y coordinate axes in which the contact problem is described. This orientation is given by angle β , as shown in Fig 2.

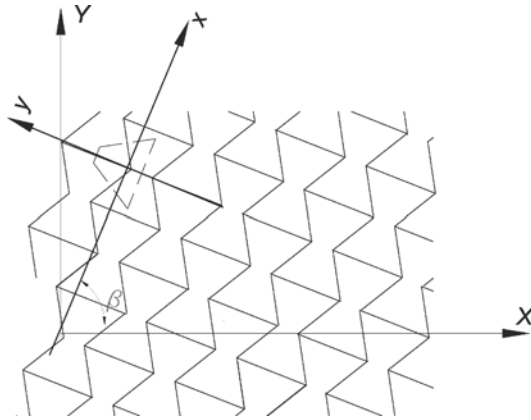


FIG. 2. Material orientation with respect to the global coordinate system.

To evaluate the energy coefficient in arbitrary point M with stress vector:

$$(3.17) \quad \boldsymbol{\sigma}^{(M)} = \left(\sigma_X^{(M)}, \sigma_Y^{(M)}, \sqrt{2}\sigma_{XY}^{(M)} \right)$$

it is necessary to decompose it into stress eigenstates. As a result, the stress vector for point M can be expressed as a linear combination of limit eigenstresses as written below:

$$(3.18) \quad \boldsymbol{\sigma}^{(M)} = A^{\text{I}} \boldsymbol{\sigma}^{\text{gr}} + B^{\text{II}} \boldsymbol{\sigma}^{\text{gr}} + C^{\text{III}} \boldsymbol{\sigma}^{\text{gr}},$$

where coefficients of this combination are as follows:

$$(3.19) \quad A = \frac{\sigma_X^{(M)} \text{II} \sigma_Y^{\text{gr}} - \sigma_Y^{(M)} \text{II} \sigma_X^{\text{gr}}}{\text{I} \sigma_X^{\text{gr}} \text{II} \sigma_Y^{\text{gr}} - \text{II} \sigma_X^{\text{gr}} \text{I} \sigma_Y^{\text{gr}}}, \quad B = \frac{\sigma_Y^{(M)} \text{I} \sigma_X^{\text{gr}} - \sigma_X^{(M)} \text{I} \sigma_Y^{\text{gr}}}{\text{I} \sigma_X^{\text{gr}} \text{II} \sigma_Y^{\text{gr}} - \text{II} \sigma_X^{\text{gr}} \text{I} \sigma_Y^{\text{gr}}},$$

$$C = \frac{\sigma_{XY}^{(M)}}{\text{III} \sigma_{XY}^{\text{gr}}}.$$

The energy coefficient is expressed by relation:

$$\varphi = A^2 + B^2 + C^2 \leq 1$$

which gives the following condition:

$$(3.20) \quad \varphi = d_1 \left(\sigma_X^{(M)} \right)^2 + d_2 \left(\sigma_Y^{(M)} \right)^2 + d_3 \left(\sigma_{XY}^{(M)} \right)^2 + d_4 \left(\sigma_X^{(M)} \sigma_Y^{(M)} \right) + d_5 \left(\sigma_X^{(M)} \sigma_{XY}^{(M)} \right) + d_6 \left(\sigma_Y^{(M)} \sigma_{XY}^{(M)} \right) \leq 1,$$

where:

$$d_1 = 0.25 \left[\left(\frac{1}{m_1} \right)^2 + \left(\frac{\cos 2\beta}{m_2} \right)^2 + \left(\frac{\sin 2\beta}{m_3} \right)^2 \right], \quad d_2 = d_1,$$

$$d_3 = \left[\left(\frac{\sin 2\beta}{m_2} \right)^2 + \left(\frac{\cos 2\beta}{m_3} \right)^2 \right],$$

$$d_4 = 0.5 \left[\left(\frac{1}{m_1} \right)^2 - \left(\frac{\cos 2\beta}{m_2} \right)^2 - \left(\frac{\sin 2\beta}{m_3} \right)^2 \right],$$

$$d_5 = 0.5 \sin 4\beta \left[\left(\frac{1}{m_2} \right)^2 + \left(\frac{1}{m_3} \right)^2 \right], \quad d_6 = -d_5,$$

$$m_1 = \lambda_1 k_1, \quad m_2 = \lambda_2 k_2, \quad m_3 = \lambda_3 k_3 / \sqrt{2}$$

and β is the angle shown in Fig. 2.

4. NUMERICAL ANALYSIS

Calculations of stiffness matrices and energy strength coefficients (material parameters) for the considered anisotropic materials are performed independently on a microstructural level by considering the strain-stress relations for a unit cell. Analytical formulae for stiffness matrices coefficients and critical energies for structures a), b), c) are obtained with application of symbolic operations provided by the Mathcad program. For structure d) the relevant description can be obtained numerically by means of FEM system.

Subsequently, those parameters were used in the FEM analysis (with ANSYS software) of numerical examples presented below.

All examples deal with a rectangular prism in plane state of strain, in rough contact with stiff flat foundation. Simple geometry and load enable to analyze the influence of microstructure type on the deformation, contact stresses and distribution of material strength coefficient.

4.1. Square block made of material with different cell types under pressure

A square block of dimensions $B \times H = 1 \times 1$ m in contact with a stiff foundation is analysed. The contact is rough with coefficient of friction $\mu = 0.3$. Pressure $p = 25$ kN/m is applied to upper edge of the block (see Fig. 3).

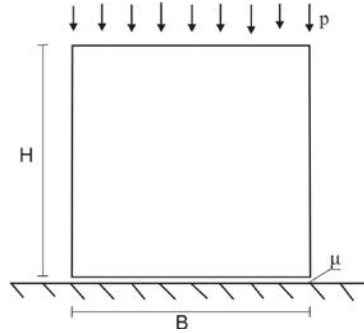


FIG. 3. Geometry and load for numerical examples.

Materials of all the types of microstructure presented above are considered. The skeleton material data are: $E_S = 10$ GPa, $\nu_S = 0.3$, $R_e = 10$ MPa and the geometric parameters are chosen to obtain the same relative material density $\rho = 0.1154$ of anisotropic cellular media in all cases. Table 1 shows specification of geometrical parameters for unit cells. Notation of the types of microstructures are the same as in Fig. 1.

Table 1. Specification of unit cells.

Structure type	Geometric parameters of skeleton [mm]	Skeleton beam thickness t [mm]
a)	$L_{01} = L_{02} = L_{03} = L_{04} = 2.6$	0.15
b)	$L_{01} = L_{02} = L_{03} = L_{04} = L_{05} = L_{06} = 1.5$	0.15
c)	$L_{01} = L_{02} = L_{03} = 4.5$	0.15
d)	$L_{01} = L_{02} = L_{03} = 3.15 \quad \gamma = 70^\circ$	0.15

Resultant macroscopic material constants are given in Table 2.

Table 2. Anisotropic material constants for cellular materials of different cell types.

Structure type	E_X [MPa]	E_Y [MPa]	ν_{XY}	ν_{YX}
a) $\beta = 0$	576.92	576.92	0.0	0.0
b)	21.87	21.87	0.96	0.96
c)	385.47	385.47	0.33	0.33
d) $\beta = 90^\circ$	0.13	1.95	-0.26	-3.85

Analysis of Table 2 leads to the conclusion that macroscopic material constants depend on the type of cellular structure. Resultant Young's moduli are the greatest for structures a) and c), smaller for honeycomb structure b) and by several orders smaller for the re-entrant structure d). Materials of structures b) and c) are isotropic and have positive Poisson's ratio. Material of structure a) has zero Poisson's ratios and structure d) produces negative Poisson's ratios, when unit cell axis are placed parallel to the coordinate frame.

The contact problem with application to the described cellular solids is solved. Figure 4 shows deformations of a square block for different materials.

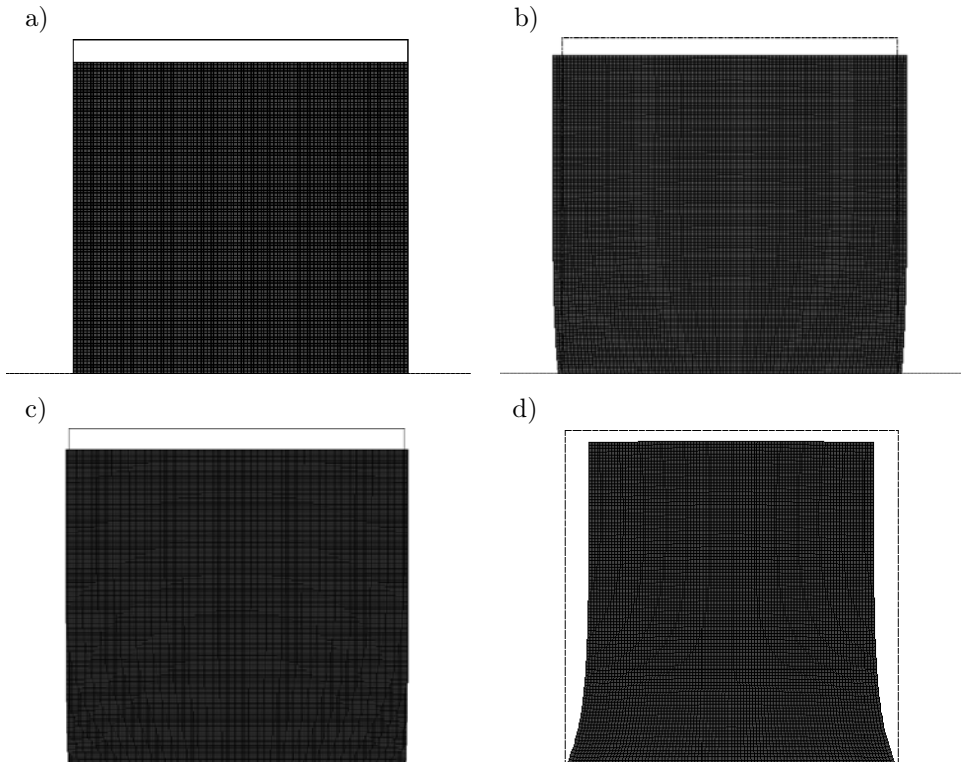


FIG. 4. Deformation of a square block of cellular material: a) square cell (material a) displacement scale 1500, b) honeycomb cell (material b) displacement scale 50, c) triangle (material c) displacement scale 1000, d) re-entrant (material d) displacement scale 3.

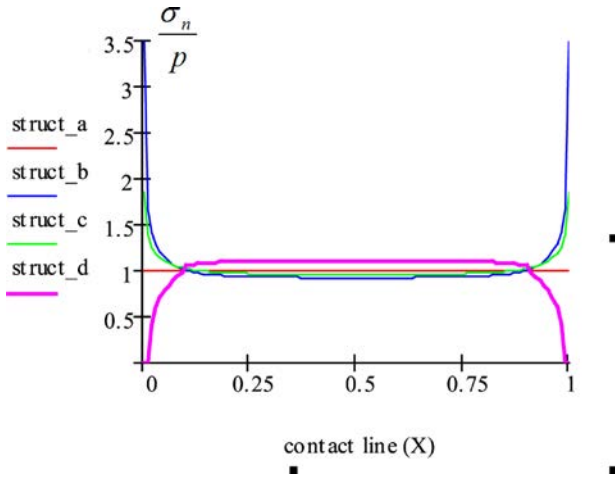
Differences in deformation types for structures with positive, zero, and negative Poisson's ratios can be observed.

Figures 5 and 6, show the relative contact pressure, friction stress distribution and contact status along the contact line.

It can be clearly seen from Fig. 5 that the most advantageous contact stress distributions correspond to a material with nonpositive Poisson's ratio. For material a) characterized by $\nu_{XY} = 0$, contact pressure is constant and friction

stress vanishes. For structure d) with $\nu_{XY} < 0$ contact pressure is homogenous in the centre of contact zone, and decreasing near the edges. Friction stress maximum appears at the point where slip begins. Figure 6 shows contact separation at the corners for this material. Structures b) and c), characterized by positive, constant ν , show the well-known pick contact pressure and friction force at the corners of the contact zone. This concentration is much greater for structure b) with ν equal to 0.96 in comparison to material with c) structure where ν attains the value 0.3.

a)



b)

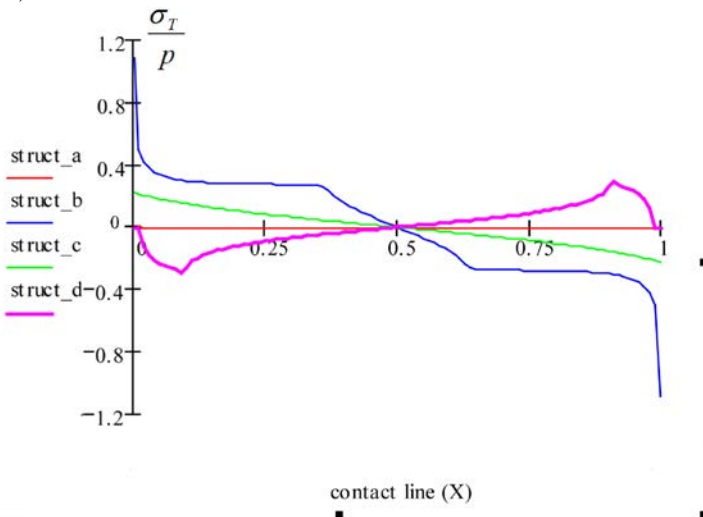


FIG. 5. Contact pressure and friction stress distribution along the contact line for different cell types.

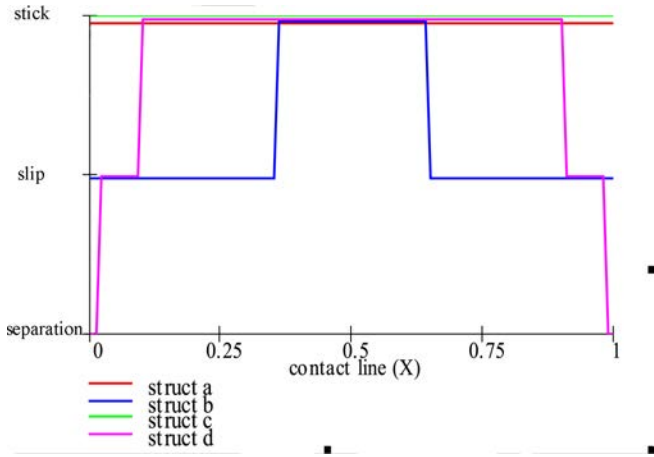


FIG. 6. Contact status (stick slip and separation zones) for different cell types.

During calculations, the energy-based yield criterion (3.20) is checked to ensure work in elastic range. Distribution of material strength coefficient for materials with structures b), c), and d) are shown in Fig. 7. For material with structure a) the value of this coefficient is constant ($\varphi = 1.0E-5$). Vanishing of

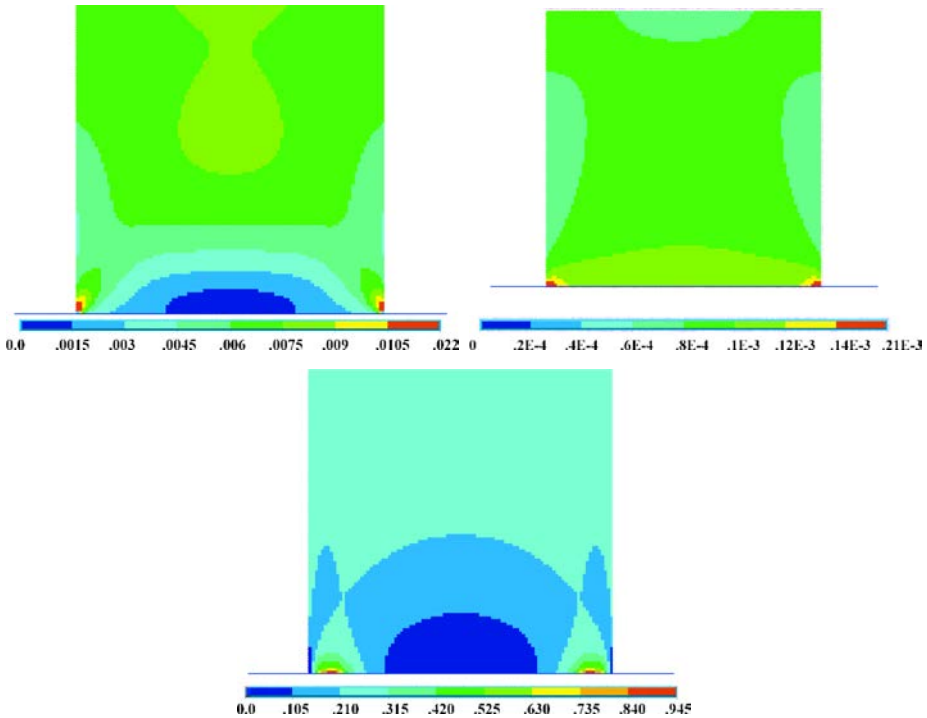


FIG. 7. Distribution of the material strength coefficient for material of structures b), c), d).

Poisson's ratio results in the lack of friction in this loading case. For structures with positive Poisson's ratio, the material strength coefficient reaches maximum in the corners of contact surface as a result of peak contact pressure. Points with maximum coefficient for structure d) correspond with maximum friction force. Reduction of the material strength in the center of contact area for structures b) and d) can be explained by energy considerations in microscale.

For the considered cellular materials, the results of numerical calculations are summarised in Table 3. The last column of this table presents the ratio of applied pressure to the admissible vertical load in nonfrictional case ($p/p_{y \max}$) for estimation of applicability of the chosen material to the given contact problem.

Table 3. Results for different cell types

Structure type	$\sigma_{n \max}/p$	$\sigma_{t \max}/p$	φ_{\max}	$p/p_{y \max}$
a)	1	0	0.00001	0.004
b)	3.6	1.08	0.022	0.083
c)	1.85	0.23	0.0002	0.009
d)	1.09	0.28	0.95	0.492

4.2. Square block made of re-entrant cellular material with different location of cell axis with respect to the contact line

Square block with geometry and contact data as in Example 4.1 with pressure $p = 4 \text{ kN/m}$ applied to its upper edge is analyzed. The block is made of re-entrant cell structure d) with skeleton material data and geometry of the unit cell as in Table 1, but with different placing of the cell symmetry axis with respect to the global coordinate system (and subsequently to body geometry, load and contact line). Calculations were made for three chosen angle values: 0, 45, and 90 degrees (see Fig. 2). Macroscopic, anisotropic material constants for those cases are presented in Table 4.

Table 4. Anisotropic material constants for different β angles.

β	E_X [MPa]	E_Y [MPa]	ν_{XY}	ν_{YX}	$p/p_{y \max}$
0	1.954	0.128	-3.85	-0.26	0.31
45	0.104	0.104	0.365	0.365	0.38
90	0.128	1.954	-0.26	-3.85	0.08

Numerical results are visualized in Figs. 8–11. The greatest vertical load capacity and the smallest Poisson's ratio $\nu_{YX} = -3.85$ correspond to the angle 90 degrees. It causes the reduction of contact pressure, and hence of the friction stress near the ends of contact line with separation at the corners. A more

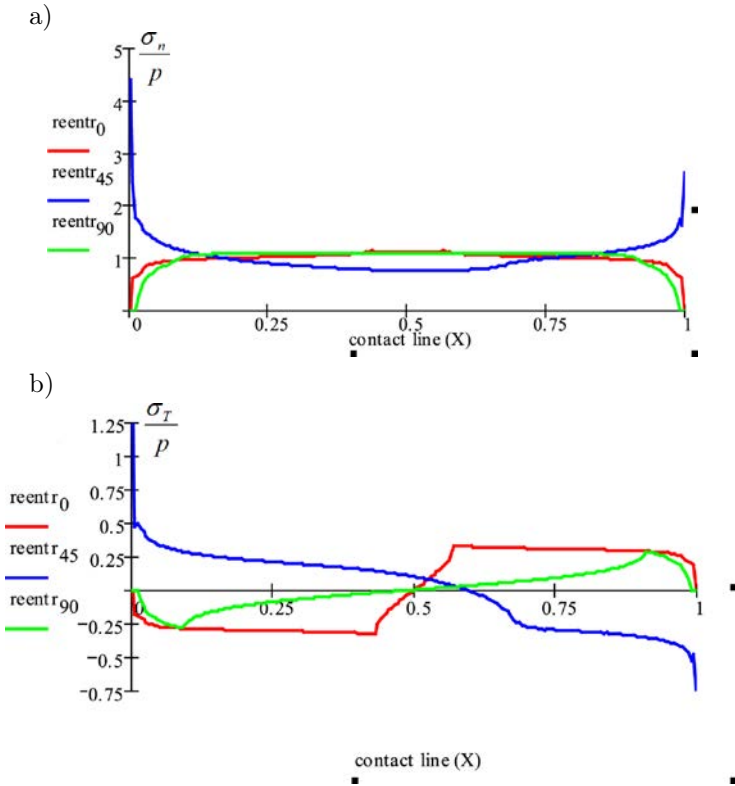


FIG. 8. Contact pressure and friction stress distribution along contact line for different reentrant cell orientation.

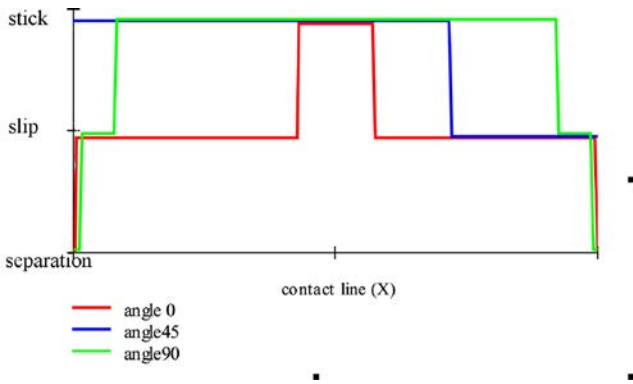


FIG. 9. Contact status (stick, slip, and separation zones) for different re-entrant cell orientation.

uniform contact pressure distribution appears for the angle of 0 degrees, with negative, but smaller absolute value of Poisson’s ratio $\nu_{XY} = -0.26$. The skew placement of the cell results in positive Poisson’s ratio, peak contact stresses at

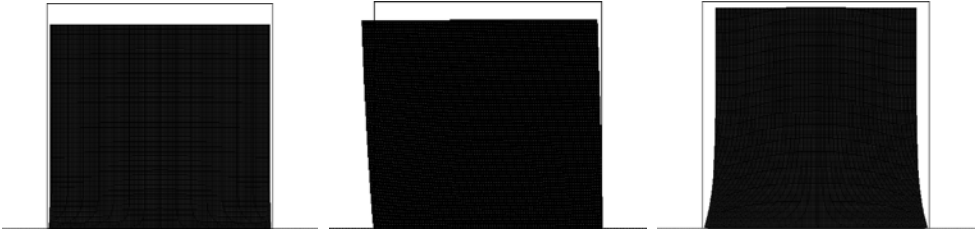


FIG. 10. Deformation of a square block made of reentrant cell microstructure for different cell orientations: $\beta = 0$ deformation scale 3, $\beta = 45$ deformation scale 2, and $\beta = 90$ deformation scale 15.

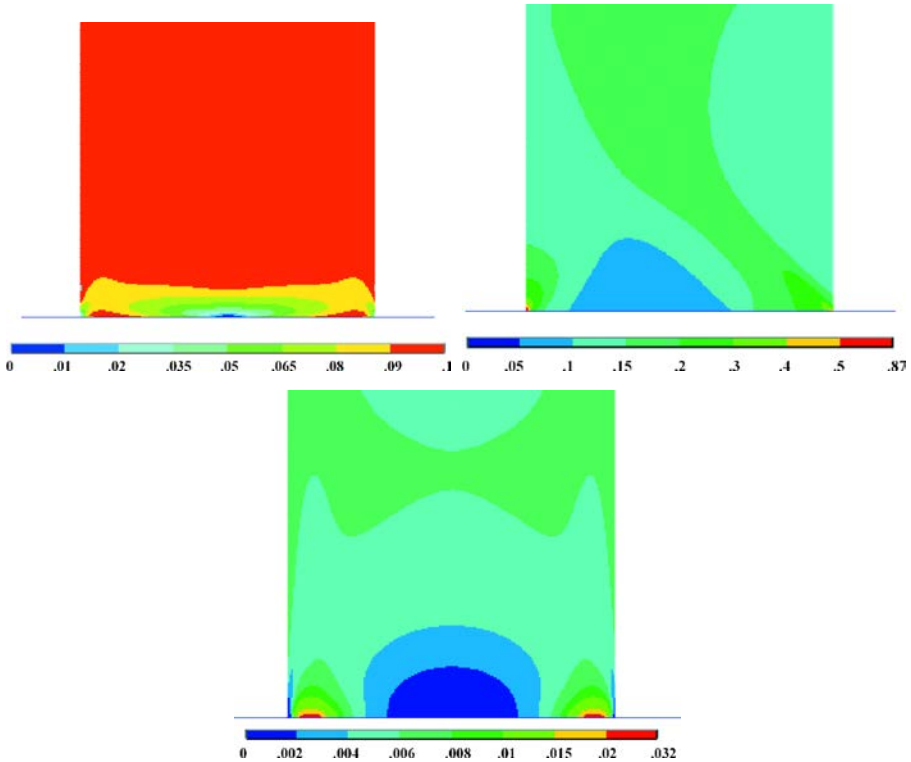


FIG. 11. Distribution of material strength coefficient for different reentrant microstructure orientation: $\beta=0$, $\beta=45$, and $\beta=90$.

the corners, and unsymmetric deformation despite the symmetric boundary conditions, due to lack of symmetry in microstructure. For 90 degrees angle, despite the smallest $\nu_{YX} = -3.85$, the stick area dominates in contact zone (Fig. 9). It is caused by domination of the resultant shear modulus over the bulk modulus. Directional proportion G/K reveals dilatational properties of the considered material and determines the relation of shear and dilatational deformation. For 0 degrees, a more uniform deformation (Fig. 10), and predominance of slip in

contact area (Fig. 9) is observed. Distributions of material strength coefficient are presented in Fig. 11. In all cases the reduction of material strength can be noticed in the center of contact zone. It can be explained by considerations on a microscale level.

4.3. Square block made of material of square cells with different locations of cell axis with respect to contact line

For comparison with the previous example, a block with the same geometry, load and boundary conditions, but made of material with structure a) (square cell) with different orientations of the cell symmetry axis with respect to global coordinate system is considered. The chosen angle values are: 0 and 45 degrees (due to structure symmetry the results for 0 and 90 degrees agree).

Material constants are given in Table 5.

Table 5. Anisotropic material constants for different β angles.

β	E_X [MPa]	E_Y [MPa]	ν_{XY}	ν_{YX}	$p_y/p_{y\ max}$
0	576.92	576.92	0	0	0.0005
45	3.795	3.795	0.99	0.99	0.018

Figures 12–15 present the results of numerical calculations.

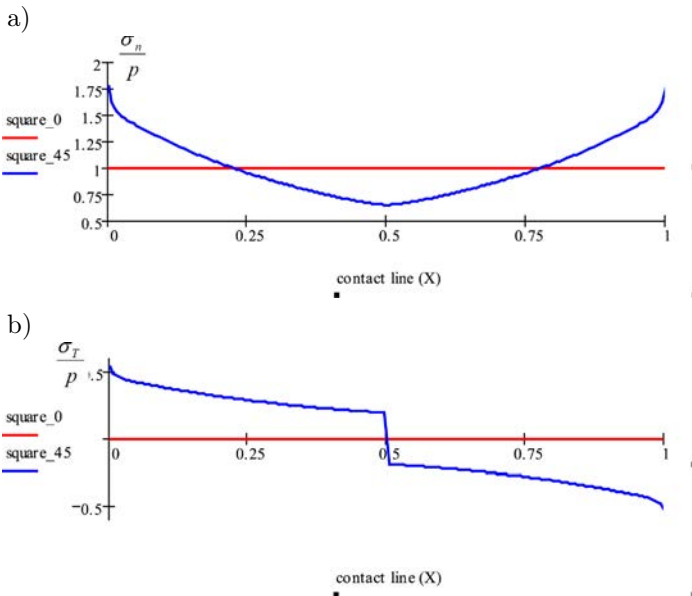


FIG. 12. Relative contact pressure and friction stresses distribution along the contact line for different square cell orientations.

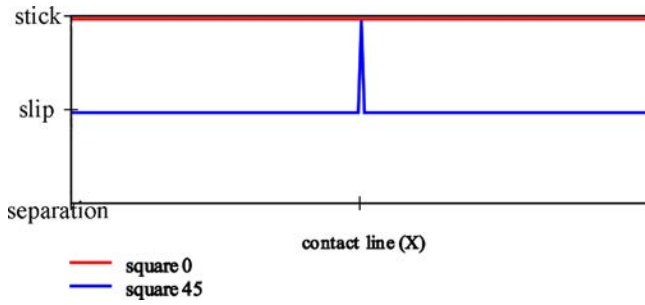


FIG. 13. Contact status (stick, slip, and separation zones) for different square cell orientations.

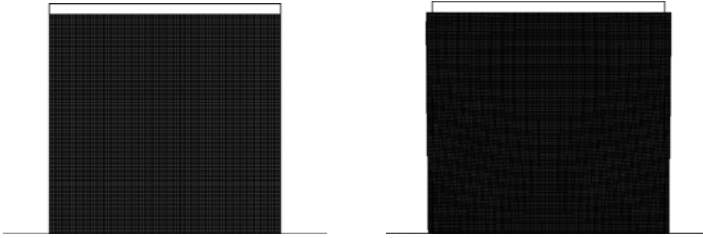


FIG. 14. Deformation of the body for different square cell orientations: $\beta = 0$ deformation scale 10000, $\beta = 45$ deformation scale 50.

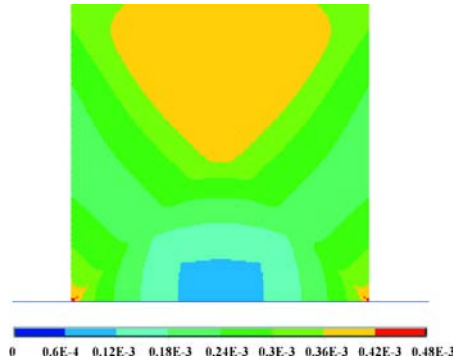


FIG. 15. Distribution of the material strength coefficient for square cell structure with orientation: $\beta = 45$.

Skew placement of the cell ($\beta = 45$) resulting in high positive Poisson's ratio leads to peaks of normal and tangential contact stresses (Figs. 12, 13), and concentration of the material strength (Fig. 15) in the corners of the contact line. Directions of reduction of the material strength coefficient for this case correspond with the maximum stiffness directions (see Appendix B). Unlike the re-entrant cell, in Example 4.2, deformation in this case is symmetrical, due to square structure symmetry for 45 degrees. For material orientation given by $\beta = 0$ ($\nu_{XY} = \nu_{YX} = 0$), the contact pressure is constant, friction stress equals

zero, and the material strength is uniform. The value of the material strength coefficient is $\varphi = 2.5\text{E-}7$.

Detailed comparison of results of the numerical examples presented above shows that stress field and contact status depend on macroscopic material properties, especially on Poisson's ratio. This ratio for cellular materials depends mainly on the topology of microstructure. The analysed structures of types b) and c) give isotropic material with positive Poisson's ratio and hence high peak contact pressure and friction stresses.

Structure d) (re-entrant) gives a compliant material with negative Poisson's ratios for a broad range of angles ($\beta \in (-18^\circ, 18^\circ) \cup (72^\circ, 108^\circ)$) (see Appendix B, point d). So the assumption that deformation at small strains does not influence the material properties can be adopted in this case. Such a material with proper placement with respect to the contact line can produce advantageous contact pressure distributions with reductions in the corners of the contact area.

Structure a), with cell symmetry axis parallel to contact line, gives a very stiff material with zero Poisson's ratio. It might seem to be most advantageous for the class of contact problems presented above (with loads perpendicular to the contact line and hence without global sliding), because it produces uniform contact pressure and zero friction stress. However it is worth to notice that material of structure a) has zero Poisson's ratio, only for unit cell placed exactly parallel to the coordinate frame. Graph of dependence of ν_{XY} on the angle of cell orientation shows that for all angles other than 0 and 90, the Poisson's ratio is positive and can reach high values, even in the close neighbourhood of 0 and 90 (see Appendix B, point a). The assumption, typical for linear analysis, that initial configuration of the structure is the reference configuration may be inappropriate in this case. It may cause that advantageous properties of the material can be overestimated. Real contact properties, especially for materials with Poisson's ratio very sensitive to cell orientation, should be obtained as a result of full nonlinear analysis, in which anisotropic effective properties of material are dependent on local configuration of the deformed body.

5. CONCLUSIONS

An analysis of static contact of cellular solid with rough stiff foundation is undertaken. Micromechanical model of cellular material is applied to predict mechanical properties on a macroscale. The study is focused on prediction of the stress distribution in contact zone and the material strength in the elastic range. Cellular materials, due to a variety of structure topology, what results in different types of material symmetry and macroscopic properties, can be tailored to special demands of the given problem. The example of contact shows that differences in behaviour can be essential and clearly visible. Special attention is paid to materi-

als with anisotropic properties, especially to materials with re-entrant structure, which give negative Poisson's ratio in a certain range of directions. Proper choice of microstructural geometrical parameters can determine the expected elastic properties. These properties and the orientation of material symmetry axis with respect to the load direction can significantly influence the contact stress distribution and may play an important role in reducing the contact peak pressure. Comparison of a material with square cells with a material of re-entrant structure allows to point out a more advantageous type of microstructure by discussion of the influence of directional material properties on the results of given example.

The contact mechanics of cellular materials is important for their friction and wear behaviour and also, under static conditions, in applications as antivibrating supports. The first topic requires consideration on a microscale and with the two-scale modelling approach can be promising area for research. The second topic requires analysis on a macro scale. The work on this problem started in this paper can be developed.

APPENDIX A.

STIFFNESS MATRICES, KELVIN MODULI, EIGENSTATES AND CRITICAL ENERGIES

Notation: \mathbf{S} – stiffness matrix, λ_α – eigenvalues of \mathbf{S} , ${}^\alpha\tilde{\boldsymbol{\varepsilon}}$ – strain eigenstates, k_α – scalar multiplier for critical eigenstate, ${}^\alpha\Phi_E^{\text{gr}}$ – critical energies in eigenstates, $\alpha = \text{I, II, III}$. L, h, t, γ – microstructural parameters (Fig. 1), E_s, v_s, R_e – skeleton material parameters.

a) Square cell structure

$$\mathbf{S} = \begin{bmatrix} \frac{E_s t}{L} & 0 & 0 \\ 0 & \frac{E_s t}{L} & 0 \\ 0 & 0 & \frac{E_s t^3}{L^3} \end{bmatrix},$$

$$\lambda_{\text{I}} = \frac{E_s t}{2l_i},$$

$$\lambda_{\text{II}} = \frac{E_s t}{2l_i},$$

$$\lambda_{\text{III}} = \frac{E_s t^3}{8l_i^3},$$

$${}^{\text{I}}\tilde{\boldsymbol{\varepsilon}} = (1, 1, 0),$$

$${}^{\text{II}}\tilde{\boldsymbol{\varepsilon}} = (1, -1, 0),$$

$${}^{\text{III}}\tilde{\boldsymbol{\varepsilon}} = (0, 0, 1),$$

$$k_{\text{I}} = \frac{R_e}{E_s},$$

$$k_{\text{II}} = \frac{R_e}{E_s},$$

$$k_{\text{III}} = \frac{R_e}{E_s} \frac{2\sqrt{2}l_i}{3t},$$

$${}^{\text{I}}\Phi_E^{\text{gr}} = \frac{R_e^2 t}{E_s 2l_i},$$

$${}^{\text{II}}\Phi_E^{\text{gr}} = \frac{R_e^2 t}{E_s 2l_i},$$

$${}^{\text{III}}\Phi_E^{\text{gr}} = \frac{R_e^2 t}{E_s 9l_i},$$

$$2l_i = L,$$

b) honeycomb structure

$$\mathbf{S} = \begin{bmatrix} \frac{\sqrt{3}E_s t (L^2 + 3t^2)}{6L (L^2 + t^2)} & \frac{\sqrt{3}E_s t (L^2 - t^2)}{6L (L^2 + t^2)} & 0 \\ \frac{\sqrt{3}E_s t (L^2 - t^2)}{6L (L^2 + t^2)} & \frac{\sqrt{3}E_s t (L^2 + 3t^2)}{6L (L^2 + t^2)} & 0 \\ 0 & 0 & \frac{\sqrt{3}E_s t^3}{3L (L^2 + t^2)} \end{bmatrix},$$

$$\lambda_{\text{I}} = \frac{\sqrt{3}}{6} \frac{E_s t}{l_i}, \quad \lambda_{\text{II}} = \lambda_{\text{III}} = \frac{\sqrt{3}}{3} \frac{E_s t^3}{l_i (4l_i^2 + t^2)},$$

$${}^{\text{I}}\tilde{\boldsymbol{\varepsilon}} = (1, 1, 0), \quad {}^{\text{II}}\tilde{\boldsymbol{\varepsilon}} = (1, -1, 0), \quad {}^{\text{III}}\tilde{\boldsymbol{\varepsilon}} = (0, 0, 1),$$

$$k_{\text{I}} = \frac{R_e}{E_s}, \quad k_{\text{II}} = \frac{R_e}{E_s} \frac{(4l_i^2 + t^2)}{(2l_i^2 + t^2 + 3\sqrt{3}tl_i)}, \quad k_{\text{III}} = \frac{R_e \sqrt{2} (4l_i^2 + t^2)}{E_s (6l + t) t},$$

$${}^{\text{I}}\Phi_E^{\text{gr}} = \frac{R_e^2 \sqrt{3}t}{E_s 12l_i}, \quad {}^{\text{II}}\Phi_E^{\text{gr}} = \frac{R_e^2}{E_s} \frac{\sqrt{3} (4l_i^2 + t^2) t^3}{6l_i (2l_i + t^2 + 3\sqrt{3}l_i t)^2},$$

$${}^{\text{III}}\Phi_E^{\text{gr}} = \frac{R_e^2 \sqrt{3}t (4l_i^2 + t^2)}{E_s 3l_i (6l_i + t)^2},$$

c) equilateral triangular structure

$$\mathbf{S} = \begin{bmatrix} \frac{\sqrt{3}E_s t (3L^2 + 2t^2)}{4L^3} & \frac{\sqrt{3}E_s t (L^2 - t^2)}{4L^3} & 0 \\ \frac{\sqrt{3}E_s t (L^2 - t^2)}{4L^3} & \frac{\sqrt{3}E_s t (3L^2 + 2t^2)}{4L^3} & 0 \\ 0 & 0 & \frac{\sqrt{3}E_s t}{4L} \end{bmatrix},$$

$$\lambda_{\text{I}} = \frac{\sqrt{3}}{6} \frac{E_s t}{l_i}, \quad \lambda_{\text{II}} = \lambda_{\text{III}} = \frac{\sqrt{3}}{3} \frac{E_s t^3}{l_i (4l_i^2 + t^2)},$$

$$\begin{aligned}
\text{I}\tilde{\boldsymbol{\varepsilon}} &= (1, 1, 0), & \text{II}\tilde{\boldsymbol{\varepsilon}} &= (1, -1, 0), & \text{III}\tilde{\boldsymbol{\varepsilon}} &= (0, 0, 1), \\
k_{\text{I}} &= \frac{R_e}{E_s}, & k_{\text{II}} &= \frac{R_e}{E_s} \frac{(4l_i^2 + t^2)}{(2l_i^2 + t^2 + 3\sqrt{3}tl_i)}, & k_{\text{III}} &= \frac{R_e}{E_s} \frac{\sqrt{2}(4l_i^2 + t^2)}{(6l + t)t}, \\
\text{I}\Phi_E^{\text{gr}} &= \frac{R_e^2}{E_s} \frac{\sqrt{3}(4l_i^2 + t^2)t}{64l_i^3}, & \text{II}\Phi_E^{\text{gr}} &= \frac{R_e^2}{E_s} \frac{2\sqrt{3}l_it}{(2l_i + 3\sqrt{3}t)^2}, & \text{III}\Phi_E^{\text{gr}} &= \frac{R_e^2}{E_s} \frac{\sqrt{3}l_i}{96t},
\end{aligned}$$

d) Inverted honeycomb, re-entrant structure.

$$\begin{aligned}
\mathbf{S} &= \begin{bmatrix} s_{1111} & s_{1122} & 0 \\ s_{1122} & s_{2222} & 0 \\ 0 & 0 & 2s_{1212} \end{bmatrix}, \\
\lambda_{\text{I}} &= \frac{1}{2} \left(s_{1111} + s_{2222} - \sqrt{(s_{1111} - s_{2222})^2 + 4s_{1122}^2} \right), \\
\lambda_{\text{II}} &= \frac{1}{2} \left(s_{1111} + s_{2222} + \sqrt{(s_{1111} - s_{2222})^2 + 4s_{1122}^2} \right), \\
\lambda_{\text{III}} &= 2s_{1212}, \\
\text{I}\tilde{\varepsilon}_x &= 1.0, & \text{I}\tilde{\varepsilon}_y &= \frac{\left(s_{2222} - s_{1111} - \sqrt{(s_{1111} - s_{2222})^2 + 4s_{1122}^2} \right)}{2s_{1122}}, \\
\text{I}\tilde{\varepsilon}_{xy} &= 0, \\
\text{II}\tilde{\varepsilon}_x &= 1.0, & \text{II}\tilde{\varepsilon}_y &= \frac{\left(s_{2222} - s_{1111} + \sqrt{(s_{1111} - s_{2222})^2 + 4s_{1122}^2} \right)}{2s_{1122}}, \\
\text{II}\tilde{\varepsilon}_{xy} &= 0, \\
\text{III}\tilde{\varepsilon}_x &= 0, & \text{III}\tilde{\varepsilon}_y &= 0, & \text{I}\tilde{\varepsilon}_{xy} &= 1.0.
\end{aligned}$$

\mathbf{S} , k_α , $\alpha\Phi_E^{\text{gr}}$ – obtained numerically.

APPENDIX B.

MACROSCOPIC MATERIAL PARAMETERS AND ADMISSIBLE VERTICAL PRESSURE IN UNIAXIAL TENSION IN DEPENDENCE ON THE ANGLE OF TENSION DIRECTION

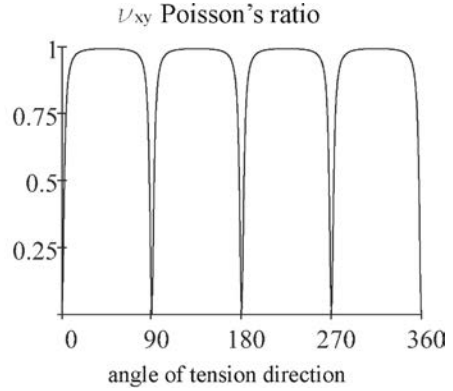
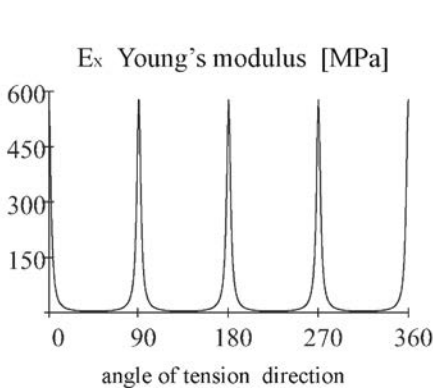
Skeleton material data: $E_S = 10$ GPa, $\nu_S = 0.3$, $R_e = 10$ MPa.
Geometrical parameters of microstructures as given in Table 1.

a) Square cell structure (anisotropic material)

analytical formula:

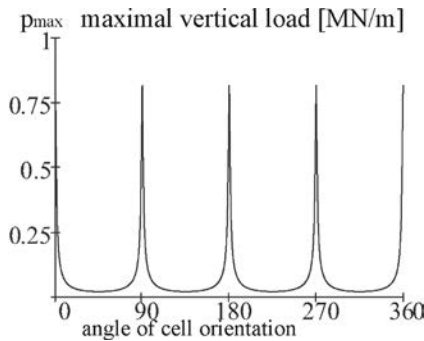
$$E = \frac{E_s t^3}{L [t^2 (1 - \sin^2 2\alpha) + L^2]}, \quad \nu = \frac{(L^2 - t^2) \sin^2 2\alpha}{[t^2 \cos^2 2\alpha + L^2]},$$

$$E_{\min} = E \left(\alpha = \frac{\pi}{4} \right) = \frac{E_s t^3}{L^3}, \quad \nu_{\max} = \nu \left(\alpha = \frac{\pi}{4} \right) = \frac{(L^2 - t^2)}{L^2},$$



analytical formula:

$$p_{\max} = \frac{4R_e t^2}{L [4t^2 (1 + \cos^2 2\beta) + 18L^2 \sin^2 2\beta]^{1/2}}.$$



b) Honeycomb structure (isotropic material)

analytical formulae:

$$E = \frac{4E_s t^3}{\sqrt{3}L [3t^2 + L^2]} = 21.87 \text{ MPa},$$

$$\nu = \frac{(L^2 - t^2)}{L^2 + 3t^2} = 0.96, \quad \nu_{\max} = \nu \left(\frac{t}{L} \rightarrow 0 \right) = 1,$$

$$p_{\max} = 0.3 \text{ MN/m.}$$

c) Equilateral triangle cell structure (isotropic material)

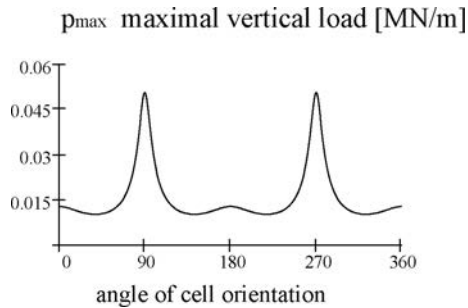
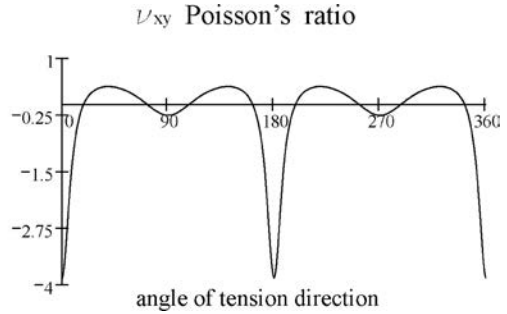
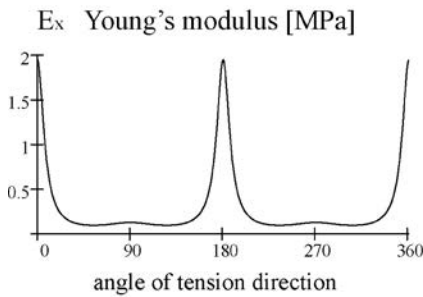
analytical formulae:

$$E = \frac{\sqrt{3}E_s t (4L^2 + t^2) (2L^2 + t^2)}{4L^3 [2t^2 + 3L^2]} = 385.47 \text{ MPa,}$$

$$\nu = \frac{L^2 - t^2}{3L^2 + 2t^2} = 0.33, \quad \nu_{\max} = \nu \left(\frac{t}{L} \rightarrow 0 \right) = 0.333,$$

$$p_{\max} = 2.77 \text{ MN/m.}$$

d) Re-entrant structure (anisotropic material)



REFERENCES

1. ANSYS 10.0 manual
2. M. JANUS-MICHALSKA, *Micromechanical model of auxetic cellular materials*, submitted for publication in Archives of Metallurgy and Materials.
3. M. JANUS-MICHALSKA, *Effective models describing elastic behaviour of cellular materials*, Archives of Metallurgy and Materials, **50**, 3, 595–608, 2005.

4. N. KIKUCHI, J. T. ODEN, *Contact problems in elasticity: a study of variational inequalities and finite element methods*, SIAM, Philadelphia 1988.
5. P. KORDZIKOWSKI, M. JANUS-MICHALSKA, R. B. PEŁCHERSKI, *Specification of energy – based criterion of elastic limit states for cellular materials*, Archives of Metallurgy and Materials, **50**, 3, 621–634, 2005.
6. R. S. LAKES, *Foam structures with a negative Poisson's ratio*, Science, **235**, 1038–1040, 1987.
7. R. S. LAKES, *Design considerations for materials with negative Poisson's ratios*, Trans. ASME J. Mech., **115**, 696–700, 1993.
8. D. W. OVERAKER, A. M. CUITINO, N. A. LANGRANA, *Elastoplastic micromechanical modeling of two-dimensional irregular convex and nonconvex (re-entrant) hexagonal foams*, Transactions of ASME, **65**, 1998.
9. A. SCALIA, *Contact Problem for porous elastic half-plane*, J. Elasticity, **60**, 91–102, 2000.
10. G. E. STAVROULAKIS, *Auxetic behavior: appearance and engineering applications*, Physica Status Solidi, **3**, 710–720, 2005.
11. G. SZEFER, D. KĘDZIOR, *Contact of elastic bodies with negative poisson's ratio*, Springer V., 2002.
12. Y. WANG, R. LAKES, *Analytical parametric analysis of the contact problem of human buttocks and negative Poisson's ratio foam cushions*, Int. J. Sol. Struc., **39**, 4825–38, 2002.
13. J. RYCHLEWSKI, *Unconventional approach to linear elasticity*, Arch. Mech., **47**, 149–171, 1995.

Received May 14, 2007; revised version February 11, 2008.
